Hollow/Rattle-Type Mesoporous Nanostructures by a Structural Difference-Based Selective Etching Strategy

Yu Chen, Hangrong Chen,* Limin Guo, Qianjun He, Feng Chen, Jian Zhou, Jingwei Feng, and Jianlin Shi*

State Key Laboratory of High Performance Ceramic and Superfine Microstructures, Shanghai Institute of Ceramics, Chinese Academy of Science, Shanghai 200050, China

ABSTRACT A novel "structural difference-based selective etching" strategy has been developed to fabricate hollow/rattle-type mesoporous nanostructures, which was achieved by making use of the structural differences, rather than traditional compositional differences, between the core and the shell of a silica core/mesoporous silica shell structure to create hollow interiors. Highly dispersed hollow mesoporous silica spheres with controllable particle/pore sizes could be synthesized by this method, which show high loading capacity (1222 mg/g) for anticancer drug (doxorubicin). Hemolyticity and cytotoxicity assays of hollow mesoporous silica spheres were conducted, and the synthesized hollow mesoporous silica spheres with large pores show ultrafast immobilization of protein-based biomolecules (hemoglobin). On the basis of this strategy, different kinds of heterogeneous rattle-type nanostructures with inorganic nanocrystals, such as Au, Fe_2O_3, and Fe_3O_4 nanoparticles, as the core and mesoporous silica as the shell were also prepared. This strategy could be extended as a general approach to synthesize various hollow/rattle-type nanostructures by creating adequate structural differences between cores and shells in core/shell structures in nanoscale.

KEYWORDS: structural difference · selective etching · homogeneous templating · hollow mesoporous silica · rattle structure · heterogeneous structure

Inorganic/organic materials with hollow interiors and well-defined morphologies in nanoscale have attracted special attention in many current and emerging areas of nanotechnology because of their unique properties, such as low density, large surface area, excellent loading capacity, high permeability, and extensive or potential applications in catalysis, chemical, or biological sensing, drug/gene storage, and controlled release.[1−9] However, traditional synthetic protocols for hollow nanostructures, such as the well-known soft/hard-templating methods,[10] Kirkendall effect,[11] galvanic replacement,[12] self-templating, and surface-protected etching,[13−15] have met limited success in the preparation of particle/pore size-controllable, morphology-controlled, and aggregation-free hollow/rattle-type mesoporous nanostructures. Traditional soft/hard-templating methods for hollow materials include the fabrication of uniform soft/hard templates and their surface functionalization followed by the deposition of heterogeneous shells. Therefore, the subsequent dissolution or calcination processes for removing the cores strongly depend on the compositional variations.[10] Herein, a novel homogeneous templating route, namely, "structural difference-based selective etching", is proposed and applied to fabricate hollow nanostructures, which is based on the creation of a unique core/shell structure where there exists distinct structural, but not compositional, differences between the interior and shell. When an appropriate etching agent is used, selective etching takes place at the interior while the outer shell remains mostly intact, and eventually a hollow structure forms. The premise for this strategy lies in the structural differences between the core and shell rather than the compositional variations. By rationally choosing the reaction components, this strategy could be employed to fabricate various kinds of hollow or rattle-type nanostructures.

In this paper, this special structural difference-based selective etching strategy has been developed to fabricate hollow/rattle-type mesoporous silica spheres, in which the silica core (as homogeneous template) was selectively etched away from the silica core/mesoporous silica shell structure while the mesoporous shell was kept almost intact. Compared to other well-developed synthetic routes to fabricate hollow mesoporous structures, this process is very simple, effective, and scalable, and the derived hollow/rattle-type mesoporous silica spheres may be more favorable in practical applications than traditional hollow/rattle-type silica spheres because of

*Address correspondence to jlshi@sunm.shcnc.ac.cn, hrchen@mail.sic.ac.cn.

Received for review October 11, 2009 and accepted December 18, 2009.

Published online December 30, 2009. 10.1021/nn901398j

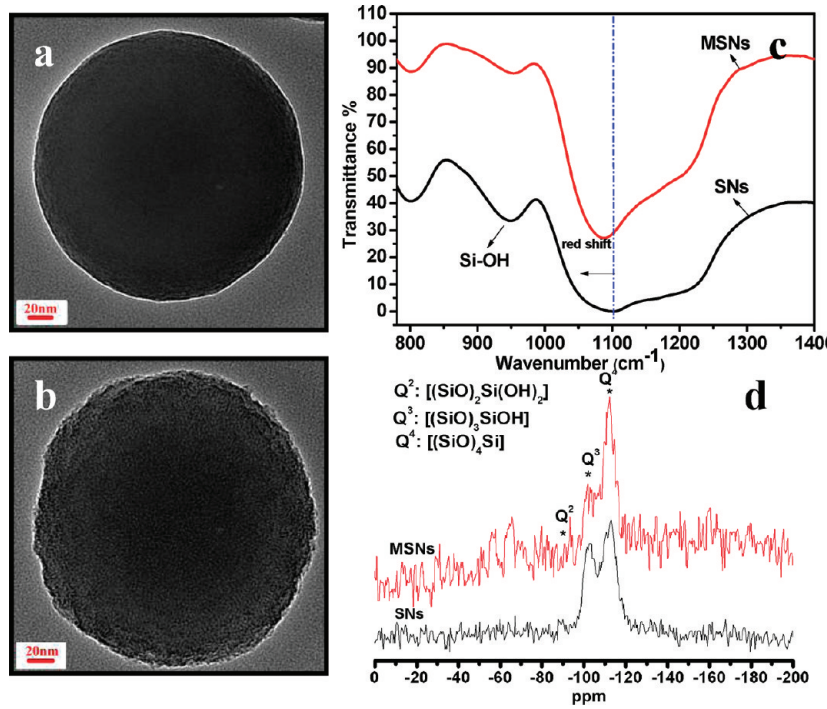

Figure 1. TEM images of SNs (a) and MSNs (b); FTIR (c) and ^{29}Si MAS NMR (d) spectra of SNs and MSNs.

the combined merits of high dispersity, uniform size distributions, tunable particle/pore sizes, and the well-defined mesoporous structure in the shell. On the basis of this strategy, we also demonstrate the successful preparation of various heterogeneous rattle-type structures with functional inorganic nanocrystals as the core (*e.g.*, Au, Fe_2O_3, and Fe_3O_4) and mesoporous silica as the shell. Because of the large surface area, high pore volume, and well-defined pore structures of obtained hollow mesoporous silica spheres (HMSs), the hemolytic-ity/cytotoxicity of HMSs (pore size = 3.6 nm), anticancer drug loading capacity, and drug release properties *in vitro* have also been explored. Besides, HMSs with large pore size (11 nm) were employed as the support for the immobilization of biomolecules (hemoglobin), which shows high loading capacity and ultrafast immobilization rate.

RESULTS AND DISCUSSION

Structural Characterization of Silica Nanospheres and Mesoporous Silica Nanospheres. Generally, monodispersed silica nanospheres (designated as SNs) with tunable particle sizes could be readily synthesized by traditional Stöber method,[16] and mesoporous silica nanospheres (designated as MSNs) are prepared by a modified conventional sol−gel method *via* adding pore-making agents such as surfactants or block copolymers in the synthetic procedures.[17] Sol−gel-derived SNs and MSNs may have structural differences between each other due to the differences in the electrostatic/covalent interactions during the hydrolysis/condensation of silicon sources under the absence/presence of structure-directing agents, such as surfactants. SNs and MSNs were prepared to demonstrate this hypothesis. For SN synthesis, tetraethyl orthosilicate (TEOS) was added into H_2O/ethanol/ammonia solution, which was hydrolyzed and condensed for 2 h. MSNs were synthesized by adding TEOS and octadecyltrimethoxysilane (C_{18}TMS, as structure-directing agent) into H_2O/ethanol/ammonia solution with the same concentration, which was hydrolyzed and condensed for 1 h.[18] Typical TEM images show that SNs and MSNs (surfactant not removed in MSNs) are of spherical morphology (Figure 1a,b), and SNs exhibit a smooth surface while MSNs show rough pore-like channels indicating the presence of micelle aggregates. The structural differences between obtained SNs and MSNs were characterized by FTIR and ^{29}Si MAS NMR techniques. Compared to that of SNs, the FTIR spectrum (Figure 1c) of MSNs shows that the transverse-optical mode of Si−O−Si asymmetric stretching vibration band exhibits a distinct red shift from 1101 to 1086 cm^{-1}. The red shift of the Si−O−Si band suggests a more open structure in MSNs, which demonstrates the higher degree of condensation of silicate species.[14,19] The intensities of Si−OH stretching vibrations (953 cm^{-1}) relative to Si−O−Si asymmetric stretching vibrations also show apparent difference between SNs and MSNs, where MSNs exhibit significantly lower relative intensity of Si−OH stretching vibrations and therefore a higher degree of condensation of the Si−O−Si network than SNs (for more direct observation, FTIR spectrum plotted in absorbance mode is given in Figure S1 in Supporting Information). To provide more direct evidence of the condensation degrees,

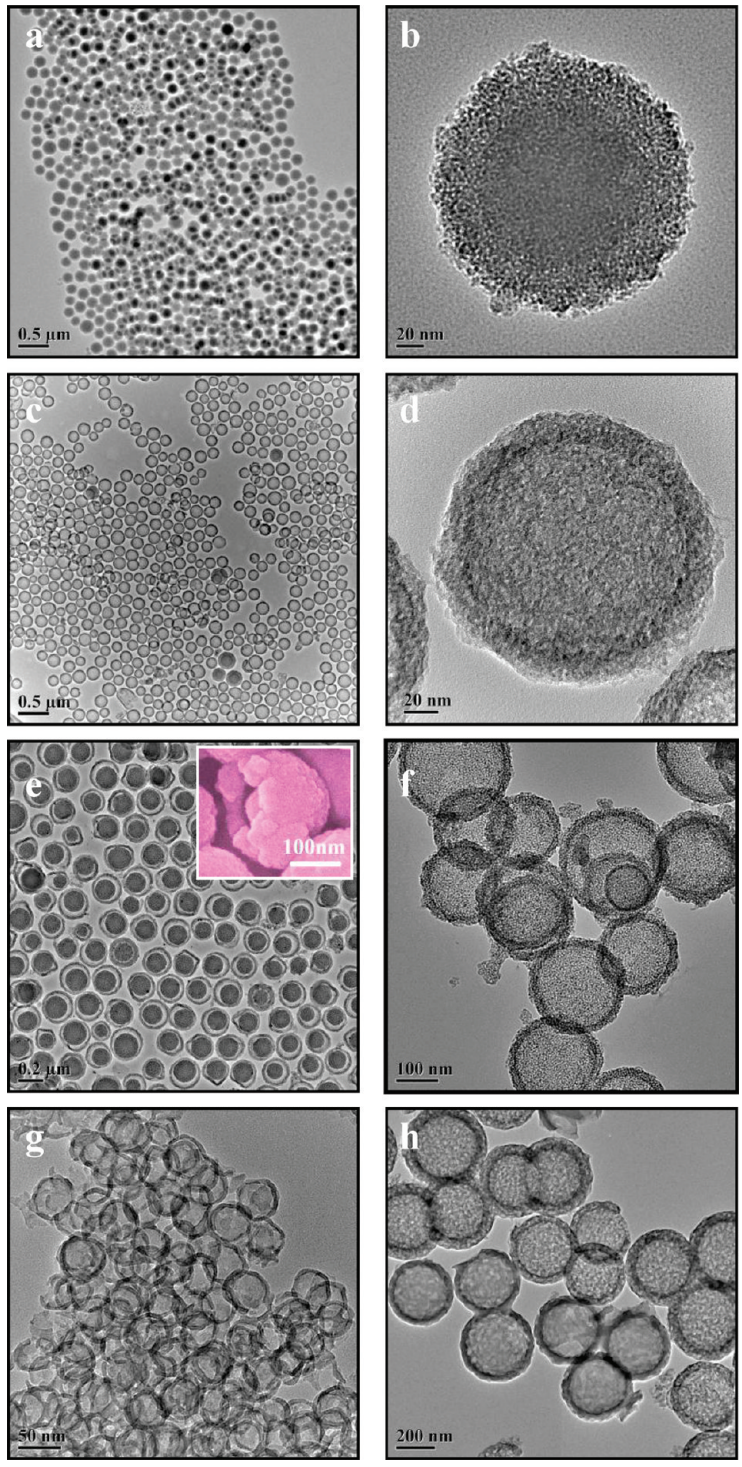

Figure 2. TEM images of $sSiO_2@mSiO_2$ (a,b); HMSs obtained by treating $sSiO_2@mSiO_2$ in 0.6 M Na_2CO_3 solution at 80 °C for 0.5 h (c,d); rattle-type and hollow mesoporous silica spheres. Inset of panel e shows SEM image of purposely selected broken rattle-type sphere, obtained by treating $sSiO_2@mSiO_2$ in 0.12 M (e) and 0.24 M (f) ammonia solution at 150 °C for 24 h. HMSs with diameters of 45 nm (g) and 450 nm (h) synthesized by using different initial precursor concentrations.

^{29}Si MAS NMR spectra of SNs and MSNs were recorded (Figure 1d), which consist of signals at −92, −101, and −111 ppm, corresponding to the Q^2 [$(SiO)_2Si(OH)_2$], Q^3 [$(SiO)_3SiOH$], and Q^4 [$(SiO)_4Si$] species, respectively. The $Q^4/(Q^2 + Q^3)$ ratio of MSNs is much higher than that of SNs, demonstrating a significantly increased number of silicon atoms fully coordinated to nearest neighbors of other silicates of MSNs as compared to that of SNs; that is, MSNs possess a much higher degree of condensation than that of SNs.[20]

Synthesis of Hollow/Rattle-Type Mesoporous Silica Spheres. If SNs and MSNs are combined to form a core/shell struc-

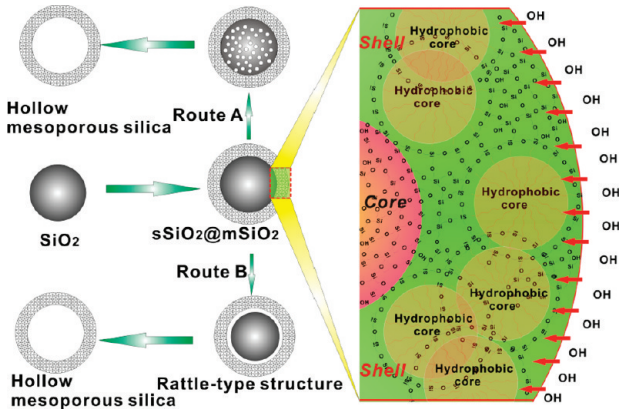

Figure 3. Formation schematics of hollow/rattle-type mesoporous silica spheres (left) and the microscopic structure schematics (right). Route A represents the selective-etching procedure in Na_2CO_3 solution and route B for that in ammonia solution under hydrothermal treatment. The local microscopic structure of the right part shows that there exist hydrophobic cores formed by the long carbon chains of C_{18}TMS, which is the pore-making area after burning out the organic carbon chains. The more open structure of the shell facilitates the penetration of the OH^- ions to selectively etch the core part, which is proved to have much more Si−OH groups than in mesoporous shell by FTIR and ^{29}Si MAS NMR spectra (Figure 1c,d).

ture, the above-mentioned structural differences may satisfy the requirements for structural difference-based selective etching strategy, which could produce hollow structure if appropriate etching agents are used. To demonstrate this assumption, solid silica core/mesoporous silica shell nanospheres (designated as $sSiO_2@mSiO_2$) were prepared by referencing the synthetic procedures for preparing SNs and MSNs to maintain the structural similarity. First, solid silica nanospheres were obtained by using ethanol/water as cosolvent and ammonia as base catalyst, which was subsequently coated with a mesoporous silica shell by the co-condensation of C_{18}TMS and TEOS. The typical TEM images of uniform $sSiO_2@mSiO_2$ core/shell structures with about 30 nm thick shells and 130 nm sized core are shown in Figure 2a,b. The obtained particles are almost perfectly spherical in shape, and there is no apparent aggregation among the particles. The pores are randomly distributed over the siliceous shell, where the core is solid and nonporous (Figure 2b). Afterward, $sSiO_2@mSiO_2$ sample was treated in a Na_2CO_3 solution before removing the surfactant. Finally, the surfactants were removed by calcination at 550 °C for 6 h. Figure 2c shows the TEM images of HMSs obtained by treating $sSiO_2@mSiO_2$ in 0.6 M Na_2CO_3 solution at 80 °C for 0.5 h. The micrograph shows that the obtained HMSs are highly dispersed and have mesoporous shells of approximately 30 nm thickness (Figure 2d).

The present structural difference-based selective etching principle can also be realized to prepare hollow or rattle-type mesoporous silica spheres from $sSiO_2@mSiO_2$ by hydrothermal treatment in ammonia solution as etching agent. When the $sSiO_2@mSiO_2$ structure was subjected to hydrothermal treatment in 0.12 M ammonia solution for 24 h at 150 °C, it could be clearly observed from the TEM image (Figure 2e) that the interspaces between the core and shell are created, resulting in homogeneous $sSiO_2@mSiO_2$ rattle-type structure. The uniform spherical morphology is also verified by SEM examinations shown in Figure S2 in Supporting Information, and the rattle-type structure is evidenced by a purposely selected broken sphere (inset of Figure 2e). Hydrothermal treatment in higher concentration ammonia solution could create HMSs (Figure 2f). Importantly, because of the mature synthetic procedure of sol−gel chemistry for controlling particle size of the silica spheres,[16] the particle sizes of HMSs could be precisely tuned by varying the initial sizes of silica core. As shown in Figure 2g,h, HMSs with particle sizes of 45 and 450 nm could be obtained simply by varying the initial precursor concentration.

Hollow Interior Evolution. Interestingly, the evolution of the hollow interior is dependent on the different selective-etching processes adopted, as schematically shown in Figure 3 for hollow interior evolutions by dissolution in Na_2CO_3 solution (route A) and by hydrothermal treatment in ammonia solution (route B). The hollow interior formation during dissolution in Na_2CO_3 solution includes the creation of small pores inside the silica core, followed by the pore growth due to the collapse of small pores to reduce the surface area.[21] However, hydrothermal treatment in water or in low concentration ammonia solution leads to the creation of cavities between the solid core and mesoporous shell. Prolonged hydrothermal treatment in higher concentration of ammonia solution can eventually lead to the formation of entirely hollow interiors. The evolution of the cavity between the core part and shell in $sSiO_2@mSiO_2$ structure is controllable by simply tuning the synthetic parameters. For example, rattle-type structures or complete hollow structures were obtained by hydrothermal treatments in ammonia solutions of different concentrations (Figure 2e,f). For another example, not all of the $sSiO_2@mSiO_2$ composite particles were converted to hollow structure within 0.5 h at 80 °C in 0.2 M Na_2CO_3 solution, as seen from the TEM image in Figure S3 in Supporting Information, where several selected particles in squares show the incomplete core removal but numerous small pores have been generated inside the core part of $sSiO_2@mSiO_2$. Furthermore, to exclude the influence of the surfactants on the etching process, the as-synthesized $sSiO_2@mSiO_2$ particles after the removal of surfactants by calcination at 550 °C were also treated in 0.6 M Na_2CO_3 solution for 0.5 h to etch away the core part. TEM image shows that the hollow interior could also be created to a certain degree in the core/shell structure (Figure S4 in Supporting Information), demonstrat-

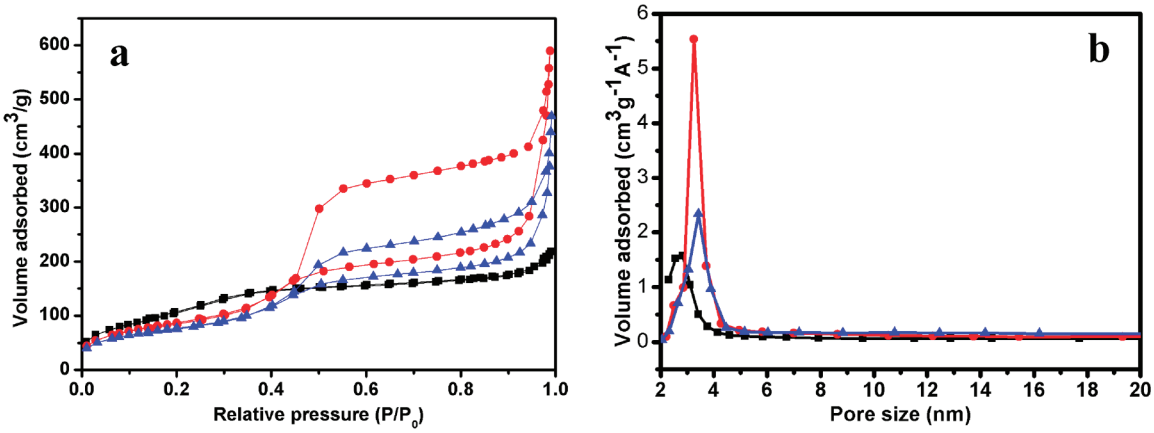

Figure 4. N_2 adsorption−desorption isotherms (a) and the corresponding pore size distributions (b) of $sSiO_2$@$mSiO_2$ (■), rattle-type mesoporous silica (●), and HMSs (▲) obtained by treating $sSiO_2$@$mSiO_2$ in 0.12 and 0.24 M ammonia solutions at 150 °C for 24 h, respectively.

ing the neglectable influence of surfactants on the evolution of hollow interior. However, calcination at high temperatures could enhance the condensation degrees of either the core or shell by decomposing the Si−OH and Si−O-R groups into Si−O−Si network and consequently diminish the difference of condensation degree of silica framework between the core and shell. Therefore, the calcined sample, especially its core, became much less dissoluble as can be seen by many remaining cores in Figure S4 in Supporting Information.

The possible reasons for the different behaviors of cavity evolution in $sSiO_2$@$mSiO_2$ between the hydrothermal treatment in ammonia and direct Na_2CO_3 dissolution may be attributed to the further condensation/polymerization of silica network under hydrothermal conditions: the further condensed SiO_2 core cannot be well dissolved in low concentration of ammonia solution or simply in water under hydrothermal treatments, but all silica cores could be dissolved by enough OH^- ions at relatively high concentration of ammonia. Comparatively, during the core dissolution by Na_2CO_3 under mild condition for a short time, numerous small pores can be generated due to the presence of extensive Si−OH and Si−O−R (R = C_2H_5 in the present case) groups within the cores, as suggested by the ^{29}Si MAS NMR and FTIR spectra in Figure 1c,d and Figure S5 in Supporting Information. Treatment for long enough time could result in the complete dissolution of the cores by OH^- ions present in Na_2CO_3 solution, while some transient states can be found by mild treatment (*e.g.*, 0.5 h, 0.2 M Na_2CO_3 solution as shown in Figure S3 in Supporting Information). According to the previous reports, selective etching of silica obtained by co-condensation between (3-aminopropyl)trimethoxysilane (APS) and TEOS or between *N*-[3-(trimethoxysilyl)propyl]ethylenediamine (TSD) and TEOS by ammonia solution or HF could create cavities to synthesize rattle-type nanostructures.[5,6,22] However, no direct evidence was provided to explain such a structural conversion in these reports.[5,6,22] Moreover, the nanopores generated by etching process were not well-defined, and the obtained nanoparticles had low surface area and pore volume.[13,22] Our developed structural difference-based selective etching strategy for mesoporous nanostructure fabrication introduced long chain silane coupling agent (C_{18}TMS) as pore-making agents in the silica shell while the dense silica core was etched away to create a hollow interior, which is substantially different from the dissolution of the middle part of co-condensed TSD and TEOS reported recently.[22] The well-defined mesopores in the shell may find broader applications than previous reports for hollow/rattle-type silica nanostructures.[5,6,13,22]

Characterization of Pore Structures. Nitrogen adsorption−desorption isothermals of $sSiO_2$@$mSiO_2$ and hollow/rattle-type mesoporous silica spheres are shown in Figure 4a, which exhibit typical Langmuir IV hysteresis, indicating the presence of well-defined mesopores. It could be observed that the isotherms of hollow/rattle-type mesoporous silica spheres show a distinctively larger hysteresis loop than that of as-prepared $sSiO_2$@$mSiO_2$, which represent ink-bottle-type pores in which larger cavities are connected by narrow windows. Calculated from the desorption branch of the nitrogen isotherm with BJH method, average pore sizes of the rattle-type and hollow mesoporous silica spheres were determined to be 3.2 and 3.4 nm, respectively, larger than that of $sSiO_2$@$mSiO_2$ (2.5 nm). It is believed that the enlargement of the pore size at increased ammonia concentrations was caused by the limited dissolution of the silica framework in the shell, which also suggests that the pore size could be tuned by adjusting the ammonia concentration used. The sharp pore size distributions of the samples (Figure 4b) indicate the well-defined mesopores existing on the shell. It is noticeable that the mesopore volume increases significantly from 0.30 to 0.66 cm^3/g when $sSiO_2$@$mSiO_2$ was hydrothermally treated in 0.12 M am-

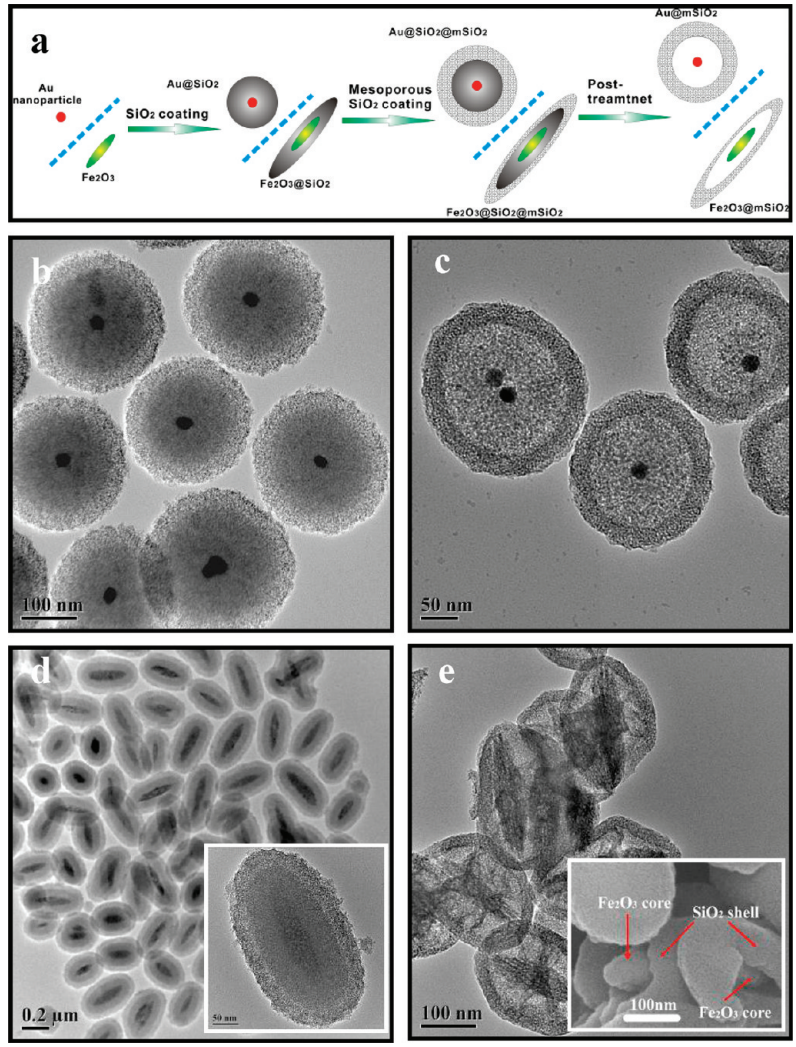

Figure 5. (a) Schematics of the synthetic procedures of heterogeneous rattle-type mesoporous nanostructures with inorganic nanocrystals (*e.g.*, spherical Au and ellipsoidal Fe_2O_3 nanoparticles) as the core and mesoporous silica as the shell; TEM images of $Au@SiO_2@mSiO_2$ (b), rattle-type $Au@mSiO_2$ (c), ellipsoidal $Fe_2O_3@SiO_2@mSiO_2$ (d and inset), rattle-type $Fe_2O_3@mSiO_2$ (e, inset: SEM image of deliberately selected broken ellipsoids).

monia solution. Apparently, the creation of large voids in the interior is responsible for the pore volume increase.

Synthesis of $Au@mSiO_2$, $Fe_2O_3@mSiO_2$, and $Fe_3O_4@mSiO_2$ Heterogeneous Structures. Our recent results have demonstrated that a novel kind of rattle-type hollow magnetic mesoporous spheres with Fe_3O_4 particles encapsulated in the hollow cores of mesoporous silica microspheres could be fabricated by sol−gel reactions on hematite particles followed by cavity generation with hydrothermal treatment and H_2 reduction.[20] The special hydrothermal treatment contributes to the cavity formation, which was caused by further condensation/densification of the middle silica layer between mesoporous silica shell and hematite core. With the present structural difference-based selective etching strategy, not only the hollow or rattle-type homogeneous silica nanostructures but also various heterogeneous rattle-type composite nanostructures with functional inorganic nanocrystals as the cores and mesoporous silica as the shell could be conveniently fabricated with a complete removal of the middle silica layer. It is known that a number of inorganic nanocrystals could be coated by silica to form core/shell structure. On this basis, we further demonstrated that heterogeneous rattle-type core/shell mesoporous nanostructures could be fabricated when a mesoporous silica shell was deposited on silica-coated nanocrystals followed by the treatment in Na_2CO_3 or ammonia solutions. As shown in Figure 5a, Au nanocrystals were synthesized by traditional sodium citrate reduction method, then a dense silica shell was coated on Au nanocrystals to form $Au@SiO_2$ core/shell structure; further, a mesoporous silica shell was introduced to form an $Au@SiO_2@mSiO_2$ structure (Figure 5b). Afterward, the composite particles could be converted to rattle-type nanostructure by mixing them into a Na_2CO_3 solution (Figures 5c and 6a,b, BET surface area = 297 m^2/g; pore volume = 0.48 cm^3/g; pore size

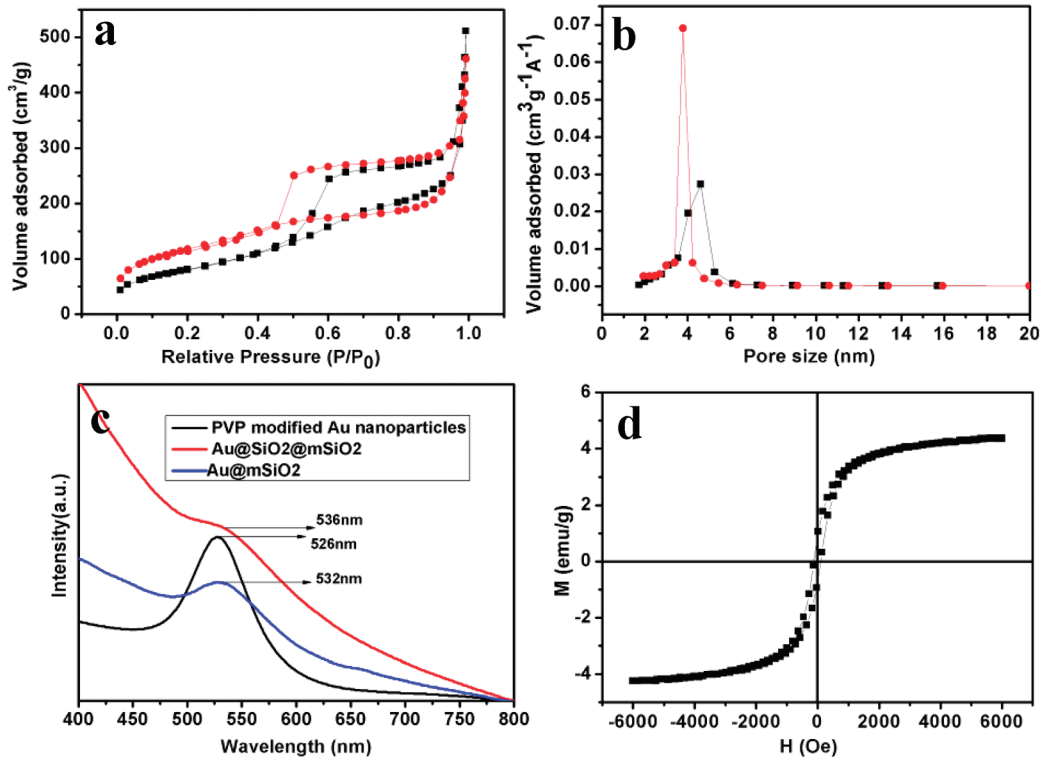

Figure 6. (a) N_2 adsorption−desorption isotherms and (b) corresponding pore size distributions of $Au@mSiO_2$ (■) and $Fe_2O_3@mSiO_2$ (●); (c) UV−vis spectra of PVP-modified Au nanoparticles, $Au@SiO_2@mSiO_2$ and $Au@mSiO_2$; (d) magnetic properties of $Fe_3O_4@mSiO_2$ after H_2 reduction.

= 4.6 nm). The successful encapsulation of Au nanoparticles within the mesoporous silica shell could also be evidenced by XRD characterization (Figure S6 in Supporting Information, JCPDS No.04-0784), which demonstrates that heterogeneous rattle-type composite nanostructures can be easily fabricated by the present strategy using the homogeneous templating technique. UV−vis spectra show that the maximum adsorption peak of $Au@SiO_2@mSiO_2$ (536 nm) exhibits a 10 nm red shift compared with that of PVP-modified Au nanoparticles (526 nm), while $Au@mSiO_2$ (532 nm) exhibits a 4 nm blue shift compared with that of $Au@SiO_2@mSiO_2$ (Figure 6c). The variation of maximum adsorption peaks is due to the changes of the local refractive index of the surrounding medium.[23] Moreover, this novel rattle-type nanostructure is of great significance in catalysis because the single encapsulation of metallic nanocrystals within a mesoporous shell could meet a number of requirements for sustained catalysis at high temperature: catalytic nanoparticles (Au nanoparticles in the present case) would not be sintered together at elevated temperatures in catalytic reactions, while the resistance to mass transfer would be minimized due to the presence of mesoporous shells in the synthesized rattle-type $Au@mSiO_2$ structure.[24,25] This $Au@mSiO_2$ rattle structure could also be used to diagnose and treat serious diseases such as cancers due to the strong plasmon-enhanced absorption and high light-scattering ability of Au for cancer diagnosis[26] and well-defined mesopores of biocompatible mesoporous silica shell for anticancer drug loading and controlled release for cancer treatment.

The present structural difference-based selective etching strategy can be also applied for fabricating nonspherical rattle-type nanostructures. For example, ellipsoidal $Fe_2O_3@SiO_2@mSiO_2$ core/shell structure was first synthesized (Figure 5a,d) and then successfully converted into rattle-type structure under hydrothermal conditions in ammonia solution (Figures 5e and 6a,b and Figure S7 in Supporting Information; BET surface area = 427 m^2/g, pore volume = 0.49 cm^3/g; pore size = 3.8 nm). SEM image of purposely selected broken ellipsoids provides direct evidence of this special rattle-type structure (inset of Figure 5e). This special structure could be applied as the magnetically targeted drug delivery vehicles after H_2 reduction to create magnetic property (Figure 6d, M = 4.36 emu/g). The large cavities between the magnetic core and mesoporous shell could store large quantities of drugs, while the mesoporous shell could exhibit sustained release profiles and the magnetic core could be used for magnetic targeting of loaded drugs, as MRI contrast agent or for hyperthermia for cancer treatment.[27−29]

Hemolyticity/Cytotoxicity Assay of HMSs, Anticancer Drug Loading/Release *In Vitro*, and Immobilization of Hemoglobin. HMSs have been adopted as the drug delivery carriers due to their large surface area, high volume, high drug loading capacity, and excellent biocompatibility.[1,2]

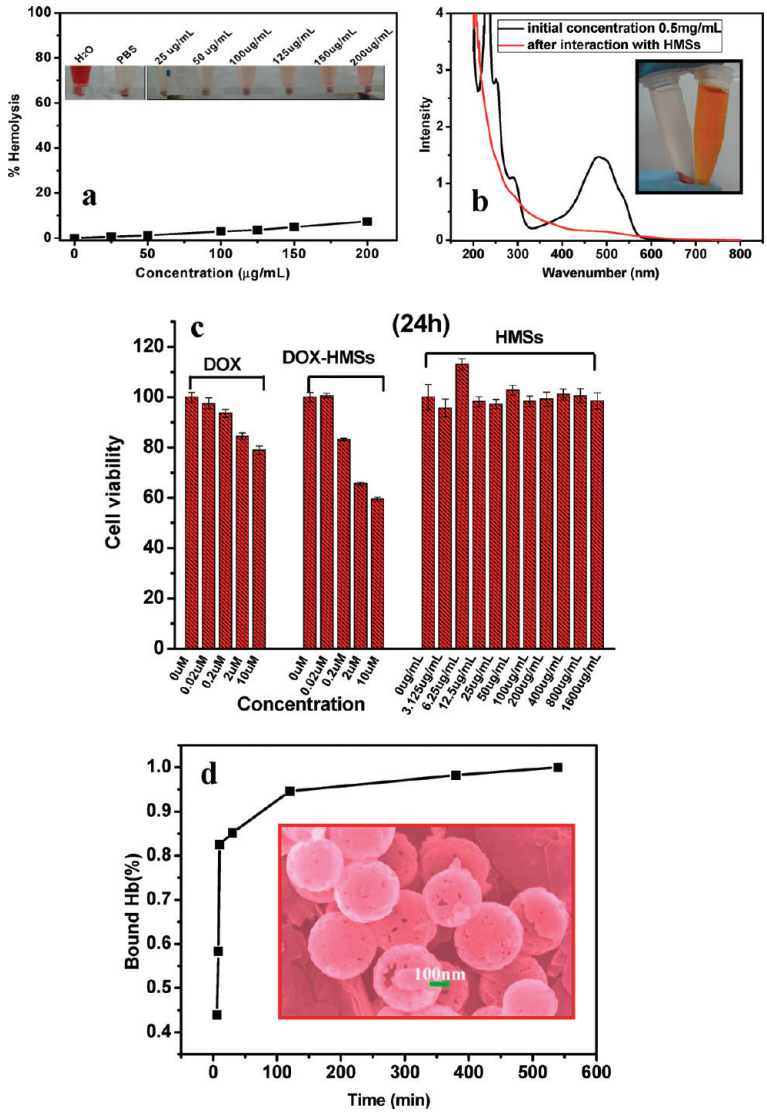

Figure 7. (a) Hemolysis assay for HMSs, using water as a positive control and PBS as a negative control (left two tubes in the inset), and the HMSs were suspended at different concentrations (right six tubes in the inset). The mixtures were centrifuged to detect the presence of hemoglobin in the supernatant visually (inset pictures of the tubes). (b) UV−vis absorbance spectra of DOX solutions before and after interaction with HMSs (inset: digital picture of DOX solution before (right) and after interaction (left) with HMSs). (c) Cell viabilities of free DOX, DOX-loaded HMSs, and HMSs at different concentrations in 24 h. (d) Adsorption amounts of hemoglobin as a function of time on HMSs with large pores (inset: SEM image of HMSs with pore sizes of 11 nm).

However, the successful intravenous injection of drug-loaded HMSs *in vivo* must guarantee the excellent blood compatibility of the carriers, such as very low hemolytic effect. To demonstrate the blood compatibility of HMSs (160 nm sized, Figure 3c), a hemolysis assay was conducted preliminarily according to the former report.[30] The red blood cell (RBC) suspensions (0.3 cm^3) were isolated from freshly obtained human blood by centrifugation and purified by successive washes with sterile isotonic phosphate buffered saline (PBS) solution. Positive and negative controls were also prepared by mixing 0.3 cm^3 of RBC suspensions with 1.2 cm^3 of deionized water and PBS, respectively. After vortexing the samples, the mixtures were allowed to stand for 2 h at room temperature. The samples were then centrifuged for 10 min at 4000 rpm. The result of hemolysis assay in the supernatant is shown in Figure 7a. The red blood cells are red due to the presence of hemoglobin in the cells. During the hemolysis assay experiments, hemoglobin will be released into the solution by hemolysis, and the resulting solution will become visually red (inset of Figure 7a) in the case of strong hemolysis. The hemolysis effect becomes visible at the increased concentrations of HMSs. However, no visible hemolysis effect can be observed visually at low concentrations of HMSs. The RBCs' hemolysis effect was further determined by measuring the absorbance of the supernatant at 541 nm (hemoglobin) by UV−vis spectroscopy (Figure S8 in Supporting Information). Approximately 7.37 and 4.91% hemolytic activities were measured at concentrations of 200 and 100 μg/mL HMSs, respectively (Figure 7a).

To evaluate the capacity as the drug delivery vehicles of HMSs, doxorubicin hydrochloride (DOX), a water-soluble anticancer drug, was loaded into HMSs. The loading efficiency of DOX is very high, which could reach 98% with the 0.5 mg/mL initial DOX concentration and 50 mg support (Figure 7b), and the drug loading content was 56 μg of DOX per 1 mg of support. The maximum loading capacity could reach 1222 mg/g (Figure S9 in Supporting Information). The positively charged DOX molecules were bonded to negatively charged support by electrostatic interaction. To demonstrate that the released DOX was pharmacologically active, the cytotoxic effect of the DOX-loaded HMSs on MCF-7 breast cancer cells was tested. Figure 7c shows cell viabilities against free DOX, DOX-loaded HMSs, and HMSs with different concentrations after cultured for 24 h. The results revealed that the cytotoxic effect of the DOX-loaded HMSs and free DOX increases with the increase of the concentration, and the DOX-loaded HMSs exhibit significantly greater cytotoxicity than free DOX (Figure 7c and Figure S10 in Supporting Information), most probably due to the inside release of DOX within the MCF-7 cells from the DOX-loaded HMSs after the uptake by the cells. The HMSs have no cytotoxicity even at the concentration of as high as 1600 μg/mL after cultured for 24 h (Figure 7c) and also neglectable cytotoxicity at 800 μg/mL for as long as 48 h (Figure S10 in Supporting Information), which shows the excellent biocompatibility of the support. Therefore, it could be concluded that HMSs have promising potentials for applications in drug loading and delivery for cancer therapy.

Mesoporous silica materials, such as SBA-15 and MSV,[31,32] have attracted much attention as promising host materials for immobilization of large molecules such as protein-based biomolecules because of their large surface areas, high pore volumes, ordered mesoporous structure, and tunable pore sizes. HMSs with large pores are an excellent candidate for the immobilization of biomolecules because the large hollow interiors could store high amount of biomolecules and thin shells could immobilize biomolecules at a fast rate.[3] However, there is no report about the immobilization of biomolecules using HMSs as the support, largely due to the synthetic difficulty for HMSs with large pores on shells. Our proposed synthetic protocol could fabricate HMSs with large pores (11 nm, inset of Figure 7d and Figure S11 in Supporting Information) simply by extending the etching time of $sSiO_2@mSiO_2$ in Na_2CO_3 solution. As shown in Figure 7d, HMSs with large pores showed an unusual ultrafast adsorption speed and high immobilization amount (310 mg/g) of biomolecules (hemoglobin). Over 85% of the hemoglobin was immobilized into HMSs within 10 min, much faster than conventional SBA-15,[30] which took more than 20 h. The fast immobilization rate could be attributed to the short mass transport path through the large pores in the thin shell of HMSs.

CONCLUSION

In summary, we have developed a facile and controllable structural difference-based selective etching strategy, which is based on the structural differences rather than traditional compositional differences, to fabricate various nanosized hollow/rattle-type mesoporous silica-based structures with tailored particle/pore sizes and morphologies by applying this novel process to solid core/mesoporous shell silica nanostructures. On the basis of this strategy, heterogeneous rattle-type nanostructures with inorganic nanocrystals, such as Au, Fe_2O_3, and Fe_3O_4 nanoparticles, as the cores and mesoporous silica as the shell were prepared. The hollow mesoporous silica spheres with different pore sizes were explored to store molecules with various sizes such as traditional anticancer drugs and biomolecules. This general strategy could be extended as a general method to synthesize other hollow/rattle-type nanostructures by rational designation in nanoscale, and the obtained nanostructures may satisfy the needs of various applications.

EXPERIMENTAL METHODS

Chemicals and Materials: Tetraethyl orthosilicate (TEOS), ethanol, Na_2CO_3, ammonia solution (25−28%), $HAuCl_4 \cdot 3H_2O$, sodium citrate, urea, NaH_2PO_4, and isopropanol were obtained from Sinopharm Chemical Reagent Co. Octadecyltrimethoxysilane (C_{18}TMS) was purchased from Tokyo Chemical Industry Co., Ltd., and polyvinylpyrrolidone (PVP10) and $Fe(ClO_4)_3 \cdot 6H_2O$ were purchased from Sigma-Aldrich. All reagents were used without further purification. Deionized water was used in all experiments.

Synthesis of SiO_2 Nanospheres (SNs) and Mesoporous SiO_2 Nanospheres (MSNs): For SNs synthesis, 6 mL of TEOS was added in the mixture of 142.8 mL of ethanol, 20 mL of H_2O, and 3.14 mL of ammonia solution, which was hydrolyzed and condensed for 2 h. For MSNs synthesis, 5 mL of TEOS and 2 mL of C_{18}TMS were mixed and added into a mixture containing 142.8 mL of ethanol, 20 mL of H_2O, and 3.14 mL of ammonia solution, which was hydrolyzed and condensed for 1 h.

Preparation of $sSiO_2@mSiO_2$: The $sSiO_2@mSiO_2$ core/shell nanoparticles (160 nm sized) were prepared by the following procedure. Typically, 142.8 mL of ethanol, 20 mL of deionized water, and 3.14 mL of ammonia solution were mixed and heated to 30 °C. Then, 6 mL of TEOS was added rapidly, and the mixture was magnetically stirred for 1 h. Five milliliters of TEOS and 2 mL of C_{18}TMS were then mixed and added into the above mixture, which was magnetically stirred for another 1 h.

Na_2CO_3 Solution Treatment of $sSiO_2@mSiO_2$ To Obtain HMSs: The as-prepared $sSiO_2@mSiO_2$ sample before the calcination of the surfactant was dispersed in 0.6 M Na_2CO_3 aqueous solution at 80 °C for 0.5 h. Then, the products were centrifuged and washed with deionized water and ethanol several times. Afterward, the products were dried at 100 °C and calcined at 550 °C for 6 h.

Hydrothermal Treatment in Ammonia Solution of $sSiO_2@mSiO_2$ To Prepare Hollow/Rattle-Type Mesoporous Silica Spheres: The as-prepared $sSiO_2@mSiO_2$ before removing the surfactant was dispersed in ammonia solution with different concentrations (0.12 and 0.24 M ammonia solution) and treated under hydrothermal conditions at 150 °C for 24 h. Then, the products were centrifuged and washed with deionized water and ethanol several times. Afterward, the products were dried at 100 °C and calcined at 550 °C for 6 h.

Hemolysis Assay: The assay experiments were carried out according to a previous report.[30] Human blood stabilized by EDTA was kindly provided by Shanghai Blood Center. The red blood cells (RBSs) were obtained by removing the serum from the blood by centrifugation and suction. After being washed with PBS solution five times, the cells were diluted to 1/10 of their volume with PBS solution; 0.3 mL of diluted RBS suspension was then mixed with (a) 1.2 mL of PBS as a negative control, (b) 1.2 mL of deionized water as a positive control, and (c) 1.2 mL of HMSs suspensions at concentrations ranging from 25 to 200 μg/mL. The mixtures were then vortexed and left to stand for 2 h at room temperature. Then, the samples were centrifuged, and the absorbance of the supernatants at 541 nm was measured by UV−vis spectroscopy.

Loading DOX into HMSs: Fifty milligrams of HMSs was mixed with 6 mL of DOX solution in PBS (0.5 mg/mL). After stirring for 24 h under dark conditions, the DOX-loaded particles were centrifuged and washed with PBS. To evaluate the DOX loading capacity, the supernatant and washed solutions were collected and the residual DOX content was measured by UV−vis measurements at a wavenumber of 480 nm. The loading efficiency (LE%) of DOX can be calculated as follows: $LE\% = ((M_{DOX1} - M_{DOX2})/M_{DOX1}) \times 100\%$, where M_{DOX1} is the original DOX content and M_{DOX2} is the remaining DOX content. To evaluate the maximum loading amount of DOX in HMSs, 1.2 mg of HMSs was mixed with 4 mL of 0.4 mg/mL DOX solution in PBS. The subsequent steps were the same as the procedures mentioned above.

***In Vitro* Cytotoxicity of HMSs and DOX-HMSs against MCF-7 Cells:** Breast cancer MCF-7 cells were seeded in a 96-well plate at a density of 2000 cells per well and cultured in 5% CO_2 at 37 °C for 24 h. Then, free DOX and DOX-HMSs were added to the medium, and the cells were incubated in 5% CO_2 at 37 °C for 24 and 48 h. The concentrations of DOX were 0.02, 0.2, 2, and 10 μM. Cell viability was determined using 3-[4,5-dimethylthiazol-2-yl]-2,5-diphenyltetrazolium bromide (MTT) reduction assay. To test the cytotoxicity of HMSs against MCF-7 cells, MCF-7 cells were seeded in a 96-well plate at a density of 10^4 cells per well and cultured in 5% CO_2 at 37 for 24 h. Then HMSs with different concen-

trations (1600, 800, 400, 200, 50, 25, 12.5, 6.25, 3.125 μg/mL) were added to the medium, and the cells were incubated in 5% CO_2 at 37 °C for 24 or 48 h. Cell viability was determined by MTT assay.

Immobilization of Biomolecules (Hemoglobin, Designated as Hb): The protein Hb immobilization method was based on the procedure reported by our previous research.[32] In a typical adsorption experiment, Hb was dissolved in potassium phosphated buffer (pH = 6.0). Kinetic experiments to determine the amount of Hb adsorbed as a function of contact time were conducted by mixing 20 mL of 1.0 mg/mL protein solution with 40 mg of hollow mesoporous silica spheres with a gentle stirring at 25 °C in a vessel sealed to prevent evaporation (initial 0.5 (w/w) hemoglobin/silica ratio). At a given time, 0.5 mL of solution was removed and then centrifuged at 10 000*g* for 3 min, followed by the extraction of upper clear solution for UV−vis spectroscopy analysis. For calculation of loading capacity of Hb, the supernatant was separated from the solid material by centrifugation, and the amount of immobilized Hb was calculated by TG characterization.

Characterization: Transmission electron microscopy (TEM) images were obtained on a JEM-2100F electron microscope operating at 200 kV. Scanning electron microscopy (SEM) images were obtained on a field emission JEOL JSM-6700F microscope. Thermogravimetry (TG) curves were recorded on a Netzsch STA 449C microanalyzer in air flow at 10 K/min. Fourier transform infrared (FTIR) spectra were obtained in the range of 400−4000 cm^{-1} using a Nicolet 7000-C with a resolution of 8 cm^{-1} by dispersing the powder samples in KBr pellets. UV−vis spectra were recorded on a UV-3101PC Shimadzu spectroscope. Nitrogen adsorption−desorption isotherms at 77 K were measured on a Micrometitics Tristar 3000 system. All samples were pretreated for 12 h at 393 K under nitrogen before measurements. The pore size distributions were calculated from desorption branches of isotherms by the Barrett−Joyner−Halenda (BJH) method. Pore volume and specific surface area were calculated by using Barrett−Joyner−Halenda (BJH) and Langmuir methods, respectively. ^{29}Si MAS NMR spectra were recorded on a Bruker AV400 (SB) spectrometer with resonance frequencies of 59.63 MHz under a magnetic field of 9.359 T. The spin rate of the sample was 4.0 kHZ, and the number of scans was 19 000−20 000. The chemical shifts were referenced to tetramethylsilane for ^{29}Si. X-ray diffraction (XRD) pattern was collected using a Rigaku D/Max-2200 PC X-ray diffractometer with Cu target (40 kV, 40 mA).

Acknowledgment. We greatly acknowledge financial support from the National Nature Science Foundation of China (Grant Nos. 20633090 and 50823007), National 863 High-Tech Program (Grant No. 2007AA03Z317), and CASKJCX Projects (Grant Nos. KJCX2-YW-M02 and KJCX2-YW-210).

Supporting Information Available: Detailed synthesis procedures (Au@$mSiO_2$, Fe_2O_3@$mSiO_2$, and Fe_3O_4@$mSiO_2$), FTIR spectra, SEM images, TEM images, XRD profiles, UV−vis spectra, cell viabilities assay, and N_2 adsorption−desorption isotherms/corresponding to pore size distributions. This material is available free of charge *via* the Internet at http://pubs.acs.org.

REFERENCES AND NOTES

1. Feng, Z. G.; Li, Y. S.; Niu, D. C.; Li, L.; Zhao, W. R.; Chen, H. R.; Gao, J. H.; Ruan, M. L.; Shi, J. L. A Facile Route to Hollow Nanospheres of Mesoporous Silica with Tunable Size. *Chem. Commun.* **2008**, 2629–2631.
2. Zhao, W. R.; Lang, M. D.; Li, Y. S.; Li, L.; Shi, J. L. Fabrication of Uniform Hollow Mesoporous Silica Spheres and Ellipsoids of Tunable Size through a Facile Hard-Templating Route. *J. Mater. Chem.* **2009**, *19*, 2778–2783.
3. Shiomi, T.; Tsunoda, T.; Kawai, A.; Matsuura, S.; Mizukami, F.; Sakaguchi, K. Synthesis of a Cagelike Hollow Aluminosilicate with Vermiculate Micro-through-Holes and Its Application to Ship-In-Bottle Encapsulation of Protein. *Small* **2009**, *5*, 67–71.
4. Lou, X. W.; Archer, L. A.; Yang, Z. C. Hollow Micro-/Nanostructures: Synthesis and Applications. *Adv. Mater.* **2008**, *20*, 3987–4019.
5. Grzelczak, M.; Correa-Duarte, M. A.; Liz-Marzán, L. M. Carbon Nanotubes Encapsulated in Wormlike Hollow Silica Shells. *Small* **2006**, *2*, 1174–1177.
6. Roca, M.; Haes, A. J. Silica-Void-Gold Nanoparticles: Temporally Stable Surface-Enhanced Raman Scattering Substrates. *J. Am. Chem. Soc.* **2008**, *130*, 14273–14279.
7. Giersig, M.; Ung, T.; Liz-Marzán, L. M.; Mulvaney, P. Direct Observation of Chemical Reactions in Silica-Coated Gold and Silver Nanoparticles. *Adv. Mater.* **1997**, *9*, 570–575.
8. Zhu, Y. F.; Kockrick, E.; Ikoma, T.; Hanagata, N.; Kaskel, S. An Efficient Route to Rattle-Type Fe_3O_4@SiO_2 Hollow Mesoporous Spheres Using Colloidal Carbon Spheres Templates. *Chem. Mater.* **2009**, *21*, 2547–2553.
9. Yi, D. K.; Lee, S. S.; Papaefthymiou, G. C.; Ying, J. Y. Nanoparticle Architectures Templated by SiO_2/Fe_2O_3 Nanocomposites. *Chem. Mater.* **2006**, *18*, 614–619.
10. Caruso, F.; Caruso, R. A.; Möhwald, H. Nanoengineering of Inorganic and Hybrid Hollow Spheres by Colloidal Templating. *Science* **1998**, *282*, 1111–1114.
11. Yin, Y. D.; Rioux, R. M.; Erdonmez, C. K.; Hughes, S.; Somorjai, G. A.; Alivisatos, A. P. Formation of Hollow Nanocrystals through the Nanoscale Kirkendall Effect. *Science* **2004**, *304*, 711–714.
12. Sun, Y. G.; Xia, Y. N. Mechanistic Study on the Replacement Reaction between Silver Nanostructures and Chloroauric Acid in Aqueous Medium. *J. Am. Chem. Soc.* **2004**, *126*, 3892–3901.
13. Zhang, Q.; Zhang, T. R.; Ge, J. P.; Yin, Y. D. Permeable Silica Shell through Surface-Protected Etching. *Nano Lett.* **2008**, *8*, 2867–2871.
14. Zhang, T. R.; Ge, J. P.; Hu, Y. X.; Zhang, Q.; Aloni, S.; Yin, Y. D. Formation of Hollow Silica Colloids through a Spontaneous Dissolution−Regrowth Process. *Angew. Chem., Int. Ed.* **2008**, *47*, 5806–5811.
15. Li, Y. S.; Shi, J. L.; Hua, Z. L.; Chen, H. R.; Ruan, M. L.; Yan, D. S. Hollow Spheres of Mesoporous Aluminosilicate with a Three-Dimensional Pore Network and Extraordinarily High Hydrothermal Stability. *Nano Lett.* **2003**, *3*, 609–612.
16. Stöber, W.; Fink, A.; Bohn, E. Controlled Growth of Monodispersed Silica Spheres in Micro Size Range. *J. Colloid Interface Sci.* **1968**, *26*, 62–69.
17. He, Q. J.; Cui, X. Z.; Cui, F. M.; Guo, L. M.; Shi, J. L. Size-Controlled Synthesis of Monodispersed Mesoporous Silica Nano-Spheres under a Neutral Condition. *Microporous Mesoporous Mater.* **2009**, *117*, 609–616.
18. Buchel, G.; Unger, K. K.; Matsumoto, A.; Tsutsumi, K. A Novel Pathway for Synthesis of Submicrometer-Size Solid Core/Mesoporous Shell Silica Spheres. *Adv. Mater.* **1998**, *10*, 1036–1038.
19. Zhu, H.; Ma, Y. G.; Fan, Y. G.; Shen, J. C. Fourier Transform Infrared Spectroscopy and Oxygen Luminescence Probing Combined Study of Modified Sol−Gel Derived Film. *Thin Solid Films* **2001**, *397*, 95–101.
20. Zhao, W. R.; Chen, H. R.; Li, Y. S.; Li, L.; Lang, M. D.; Shi, J. L. Uniform Rattle-Type Hollow Magnetic Mesoporous Spheres as Drug Delivery Carriers and Their Sustained-Release Property. *Adv. Funct. Mater.* **2008**, *18*, 2780–2788.
21. Park, S. J.; Kim, Y. J. Size-Dependent Shape Evolution of Silica Nanoparticles into Hollow Structures. *Langmuir* **2008**, *24*, 12134–12137.
22. Chen, D.; Li, L. L.; Tang, F. Q.; Qi, S. Facile and Scalable Synthesis of Tailored Silica "Nanorattle" Structures. *Adv. Mater.* **2009**, *21*, 3804–3807.
23. Liz-Marzán, L. M.; Giersig, M.; Mulvaney, P. Synthesis of Nanosized Gold−Silica Core−Shell Particles. *Langmuir* **1996**, *12*, 4329–4335.
24. Joo, S. H.; Park, J. Y.; Tsung, C. K.; Yamada, Y.; Yang, P. D.; Somorjai, G. A. Thermally Stable Pt/Mesoporous Silica Core−Shell Nanocatalysts for High-Temperature Reactions. *Nat. Mater.* **2009**, *8*, 126–131.

25. Arnal, P. M.; Comotti, M.; Schüth, F. High-Temperature-Stable Catalysts by Hollow Sphere Encapsulation. *Angew. Chem., Int. Ed.* **2006**, *45*, 8224–8227.
26. Boisselier, E.; Astruc, D. Gold Nanoparticles in Nanomedicine: Preparations, Imaging, Diagnostics, Therapies and Toxicity. *Chem. Soc. Rev.* **2009**, *38*, 1759–1782.
27. Zhao, W. R.; Gu, J. L.; Zhang, L. X.; Chen, H. R.; Shi, J. L. Fabrication of Uniform Magnetic Nanocomposite Spheres with a Magnetic Core/Mesoporous Silica Shell Structure. *J. Am. Chem. Soc.* **2005**, *127*, 8916–8917.
28. Lu, C. W.; Hung, Y.; Hsiao, J. K.; Yao, M.; Chung, T. H.; Lin, Y. S.; Wu, S. H.; Hsu, S. C.; Liu, H. M.; Mou, C. Y.; *et al.* Bifunctional Magnetic Silica Nanoparticles for Highly Efficient Human Stem Cell Labeling. *Nano Lett.* **2007**, *7*, 149–154.
29. Shi, D. L.; Cho, H. S.; Chen, Y.; Xu, H.; Gu, H. C.; Lian, J.; Wang, W.; Liu, G. K.; Huth, C.; Wang, L. M.; *et al.* Fluorescent Polystyrene−Fe_3O_4 Composite Nanospheres for *In Vivo* Imaging and Hyperthermia. *Adv. Mater.* **2009**, *21*, 2170–2173.
30. Slowing, I. I.; Wu, C. W.; Vivero-Escoto, J. L.; Lin, V. S. Y. Mesoporous Silica Nanoparticles for Reducing Hemolytic Activity towards Mammalian Red Blood Cells. *Small* **2009**, *5*, 57–62.
31. Fan, J.; Lei, J.; Wang, L. M.; Yu, C. Z.; Tu, B.; Zhao, D. Y. Rapid and High-Capacity Immobilization of Enzymes Based on Mesoporous Silicas with Controlled Morphologies. *Chem. Commun.* **2003**, 2140–2141.
32. Zhu, Y. F.; Shen, W. H.; Dong, X. P.; Shi, J. L. Immobilization of Hemoglobin on Stable Mesoporous Multilamellar Silica Vesicles and Their Activity and Stability. *J. Mater. Res.* **2005**, *20*, 2682–2690.